Computational Mechanics 26 (2000) 148–156 © Springer-Verlag 2000

A numerical algorithm for the full coupling of mechanical deformation, thermal deformation and phase transformation in surface grinding

M. Mahdi, L. Zhang

Abstract When an alloy steel experiences a critical grinding condition, irreversible deformation caused by mechanical loading, thermal loading and micro-structural phase transformation couples with strong non-linearity. This paper presents an algorithm to analyze the residual stresses induced by the full coupling of all the above causes of residual stresses involving significant temperature- and microstructure-dependent property changes of workpiece materials. User-supplied subroutines to an existing FEM code were developed to simulate the coupled effect at the resolution of integration points. Results showed that the algorithm is quite efficient and stable in dealing with the non-linearity in grinding induced deformation.

List of symbols

Cr_{700} cooling rate at 700 °C (degree/h)
c specific heat capacity per unit volume
$\mathbf{D}$ constitutive matrix
H non-dimensional heat transfer coefficient ($2\alpha h/\kappa v$)
H_V Vickers hardness
h heat transfer coefficient of coolant
L_c length of grinding zone, see Fig. 1
l_a relative peak location of a heat flux ($2\zeta_a/L_c$), see Fig. 1
M Martensite
Pe Peclet number ($vL_c/4\alpha$)
q heat flux per unit grinding width
q_a peak value of the heat flux
r the positive ratio of elastic to total strain increments, see Eq. (5)
p average normal traction intensity
p_a peak value of normal traction intensity, see Fig. 1
T temperature rise with respect to ambient temperature T_∞
t time
v moving speed of the heat source and traction, see Fig. 1
w cooling factor (Mahdi and Zhang (1997))
Y yield stress of the workmaterial
κ thermal conductivity
α thermal diffusivity
μ ratio of horizontal to vertical grinding forces
σ stress tensor

Subscripts

aust austenising
e elastic, effective
ep elastic–plastic
f finish
s start
v virgin
x, y, z x-, y-, and z-directions, see Fig. 1
y yield
∞ room temperature

1 Introduction

The rapid heating and cooling produced in a grinding process may cause phase transformation and thermal plastic deformation in a workpiece and thereby introduce substantial residual stresses. When phase transformation takes place, the properties of the workpiece material change. The extent of such change depends on the temperature history experienced and the instantaneous thermal stresses developed. To carry out a reliable residual stress analysis, therefore, a comprehensive modelling technique and a sophisticated computational procedure that can accommodate the property change of material need to be developed.

The study on the numerical treatment of phase transformation induced residual stresses by grinding is lacking. However, some investigations on relevant problems are helpful. Okamura et al. (1989) developed a method using the finite element method to analyze processes involving phase transformation for analyzing the distortion of oil-quenched gear rings. Kim et al. (1992) analyzed the transient heat flow and thermal stress during surface hardening by a modified two-dimensional finite element model. Nakasaki et al. (1997) developed and applied the finite element computer package 'HEARTS' based on the metallo-thermo-mechanics to the simulation of the quenching process of a carbon steel (S45C) by pulsed YAG laser, which allowed them to evaluate the coupled effects of phase transformation, temperature and stress. Taljat et al. (1998) developed an uncoupled thermal-mechanical finite element (FE) model that took into account the effects of liquid-to-solid and solid-state phase transformations. However, the efficiency, accuracy and stability of these

M. Mahdi (✉), L. Zhang
Department of Mechanical and Mechatronic Engineering, The University of Sydney, NSW 2006, Australia

The financial support from ARC to the present study is appreciated. ADINA code was used for all the calculations.

methods have not been detailed and their suitability to grinding analysis has never been examined.

The present study aims to present a simple and explicit numerical algorithm based on FEM to investigate the grinding-induced residual stresses associated with the full coupling of thermal deformation, mechanical deformation and phase transformation. The property changes of workpiece materials due to phase transformation and the boundary conditions of grinding zone will be taken into account using the user-supplied material options of an existing FEM code, ADINA (1992).

2
Modelling and algorithm

As shown in Fig. 1, the deformation of a workpiece subjected to a surface grinding operation is considered as a plane-strain problem, and the heat generated by grinding is approximated by a triangular heat source moving along the positive direction of x-axis on the workpiece surface (Mahdi and Zhang, 1994, 1995, 1997, 1998a; Zhang and Mahdi, 1995). The cooling of the ground surface is carried out by convection heat transfer thereby ignoring the effect of radiation that is relatively very small. The interaction grinding forces are replaced by triangular traction profile coinciding with that of the heat source (Mahdi and Zhang, 1996, 1998b) in the grinding zone (GZ) of length L_c. The workmaterial considered is EN23 steel (British Iron and Steel Research Association, 1969) whose properties are shown elsewhere (Mahdi and Zhang, 1995, 1996, 1997, 1998a, b). The mechanical deformation of the workpiece material is considered to be elastic-perfectly plastic.

2.1
Material property change due to phase transformation

When a workmaterial is subjected to grinding and experiences a critical temperature change characterized by austenising and quenching, phase change will take place (Atkin and Met, 1977). In general, martensite transformation will lead to the changes of both mechanical and thermal properties of the material. To study the residual stresses of phase transformation by the finite element method, the central step is to develop a suitable constitutive model that characterizes the behavior of the workpiece material during phase transformation.

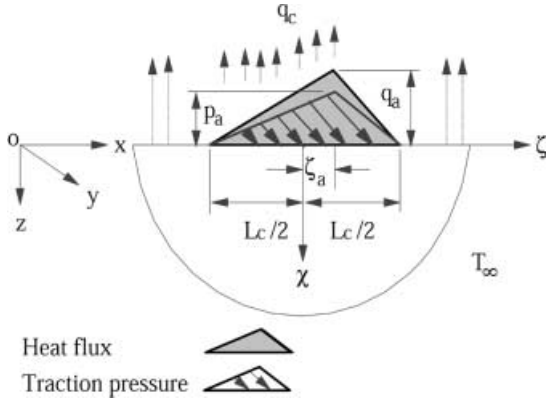

Fig. 1. The modelling of surface grinding

Table 1. The phase change properties of EN23 steel

Critical cooling time between 1029 and 773 °K	Austenizing temperature (°K)
<1.6 s	1123

The critical cooling velocity to obtain a martensitic transformation relies on the workmaterial's chemical composition. The maximum critical time to achieve martensite is given in Table 1. To have martensite transformation, the maximum ground surface temperature should be elevated to austenising temperature followed by critical cooling, which does happen in grinding. In this study, it is assumed that, the phase transformation is dependent on grinding temperature history only. Therefore the steel composition is used to determine the variation of workmaterial hardness of the finally formed martensite, i.e.

$$H_V = 463.2376 + 21 * \log(Cr_{700}) \quad (1)$$

where H_V is the Vickers hardness and Cr_{700} is the cooling rate detected at 700 °C as degree per hour. The yield stress of martensite, M_Y, can be calculated as

$$M_Y = 80.0 + 2.7544 * H_V \quad (2)$$

The yield stress of workmaterial undergoing phase transformation is approximated as a weighted average based on the percent of martensite formed, M%, that is

$$\sigma_Y = M\% * M_Y + (1 - M\%) * Y_v \quad (3)$$

where σ_Y is the instantaneous yield stress of the material undergoing phase change and Y_v is the virgin yield stress of the material before phase transformation. The percentage of martensite is related to the cooling temperature history which relies on on the starting temperature of martensite formation, M_s(300 °C) and the final temperature M_f(85 °C). The other properties are considered to be the same as that of the original workmaterial. Under slower cooling rates, a second phase change may take place in subsurface layers. However, such a phase change does not have any considerable effect on workmaterial properties and therefore is ignored in this study.

2.2
Algorithm

To build-up an adequate finite element model for a grinding process, an algorithm is required to ensure an appropriate coupling of property changes of the the material, the moving boundary conditions of the grinding zone and the control volume treatment.

2.2.1
Constitutive model

To incorporate the phase transformation relation, Eq. (1), into the stress analysis, an algorithm was designed to: (a) determine the state of grinding temperature in relation to grinding conditions, and (b) calculate the hardness and corresponding mechanical properties at a given integration point in the FEA associated with the movement of the heat source and traction. The surface cooling effect is modeled by convection heat transfer only (Mahdi and Zhang, 1995). The convection heat transfer coefficient outside GZ, h, is taken as constant. However the magni-

tude of h inside the grinding zone is scaled by a factor, w. On the other hand, the grinding temperature is also influenced by the grinding table speed which plays an important role by controlling the heat energy conducted to the ground surface. In other wards, a higher table speed results in a less time for the surface heat energy to be conducted and thereby yields lower grinding temperature if all other conditions are kept the same.

To simplify the calculation, an incremental explicit stress–strain relation is desirable. To this end, the instant workmaterial properties at each increment must be evaluated in the light of the instant stress state. For an elastic-perfectly plastic material considered here, the effective stress is either equal or less than the yield stress. However, if workmaterial undergoes critical grinding temperature history and phase change happens, the yield stress must be updated instantaneously to take into account the martensite formation.

As usual, assume that the constitutive matrix of an elastic-perfectly plastic material is **D** (Bathe, 1982). Thus for an iso-thermal elastic material, $\mathbf{D}_e$ is a constant matrix. For an elastic-perfectly plastic material, however, the constitutive matrix, $\mathbf{D}_{ep}$, is in general a highly nonlinear function of stress, strain and temperature. Prior to plastic deformation, the (trial) stress increments are related to strain increments by

$$\Delta\sigma = \mathbf{D}_e \Delta\varepsilon \tag{4}$$

If the new trial effective stress is beyond the yield stress, Eq. (4) needs to be recalculated by

$$\Delta\sigma = (\mathbf{D}_e + (1-r)\mathbf{D}_{ep})\Delta\varepsilon \tag{5}$$

where r is the positive scalar ratio of elastic to total strain increments.

According to Eq. (A9) in the appendix, there exist two values of r, whose existence indicates that either the stress increments are shortened by r_1 or inverted by r_2. Figure 2 illustrates the geometrical meaning of r_1 and r_2. With r_1, the scale ratio of stress increment a–d, the stress state moves from point a to c. However, with ratio r_2 the stress state moves to b. The distance between b and a is greater than that between c and a as r_2 is larger than r_1. The above can be more clearly demonstrated under uniaxial stress state. In this case,

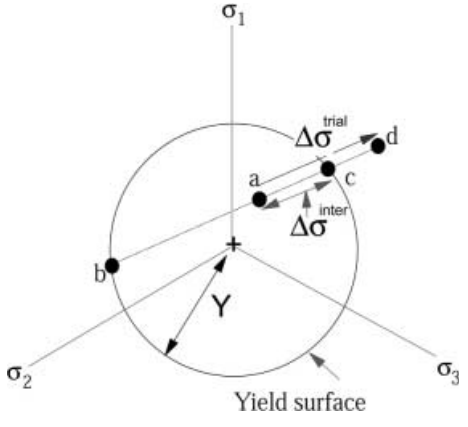

Fig. 2. Intersection of elastic stress increments and yield surface in stress space

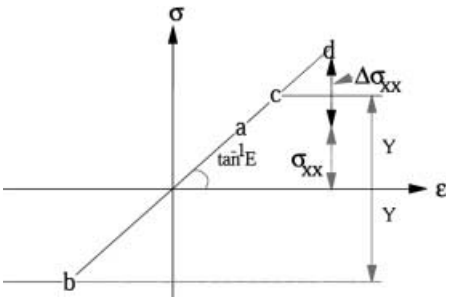

Fig. 3. Intersection of elastic stress increments with yielding in uniaxial tension

$$r_1 = (-\sigma_{xx} + Y)/(\Delta\sigma_{xx}) \quad \text{and}$$
$$r_2 = (-\sigma_{xx} - Y)/(\Delta\sigma_{xx}) \tag{6}$$

which shows that the tensile stress can be enlarged to Y or reduced to become negative Y as shown in Fig. 3. It should be noted that r_1 is always less or equal to 1 and is to be used to update elastic stress increments.

2.2.2 Verification

Although the stability of the above explicit stress integration has been investigated in particular applications (Mahdi and Zhang, 1999), its validity and accuracy with thermo-mechanical loading is further demonstrated by analyzing the deformation of a sphere under axisymmetric compression by two rigid smooth plates as shown in Fig. 4. The sphere material is elastic-perfectly plastic. Figure 4 shows that the resultant plastic zones predicted by the above algorithm and that with the standard ADINA (1992) are in close agreement with each other in terms of both size and location, under various loading conditions.

2.2.3 Boundary conditions

To represent the movement of the heat source and the change of material thermal properties, a complete algorithm has been discussed in the authors' previous work (Mahdi and Zhang, 1995). The simulation of traction movement, however, requires a more comprehensive methodology by employing the user-supplied loading option of ADINA. A code is therefore built-up to substitute the consistent forces (Bathe, 1982) directly at the finite element nodes. First, the surface node locations (yy, zz) are garbed and sorted at time = 0 to form elemental nodes. Then, the moving traction is replaced by consistent normal and tangential nodal forces on each surface node. The magnitudes of the forces are calculated for each subsequent time steps according to traction (grinding zone) location along the ground surface. The ratio of the tangential nodal force to the normal node force reflects the 'friction' which is negative for up- and positive for down-grinding respectively. When such a user-defined subroutines of moving traction are linked to the main program of ADINA, the elemental nodal force are evaluated and assembled to form the global external nodal forces. Four Gauss integration points were used to achieve this as traction profile is triangular and is a non-smooth function.

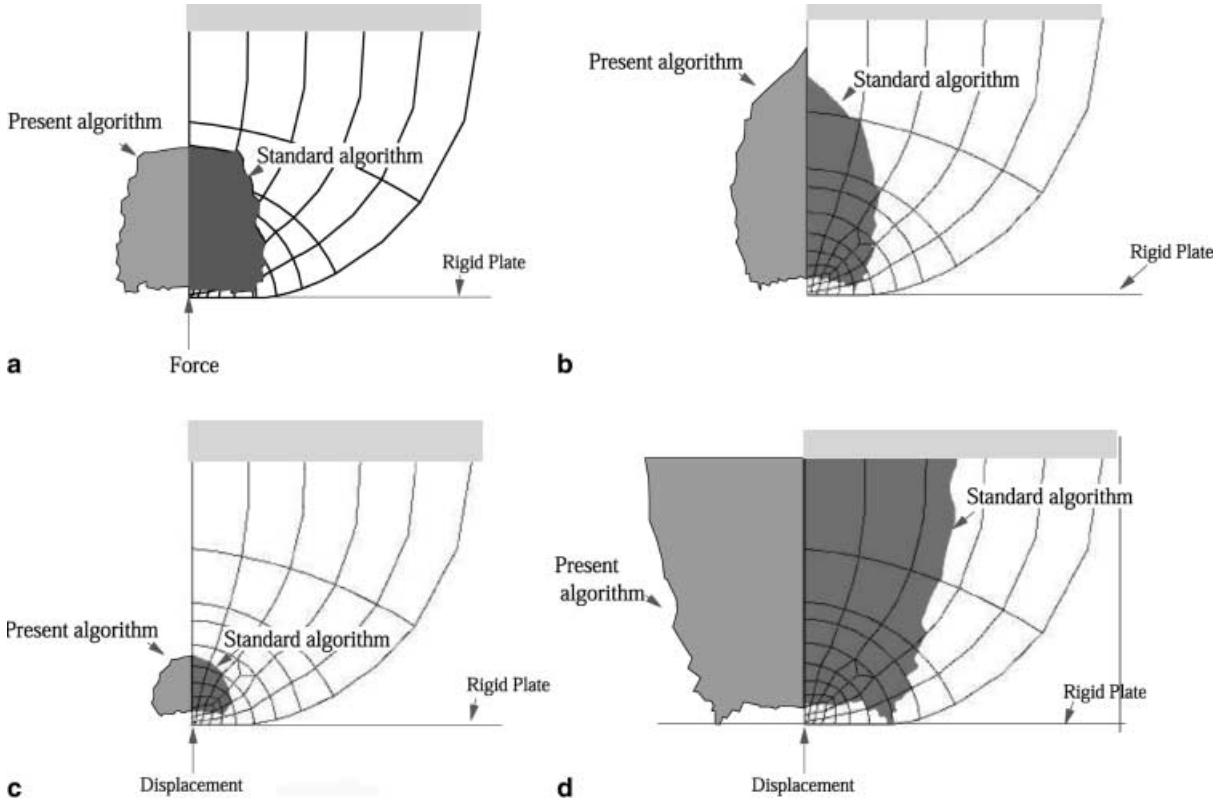

Fig. 4a–d. A comparison of the plastic zone developed in an elastic-perfectly plastic sphere compressed by two rigid smooth plates (the left is from the present algorithm and the right is from the standard implicit algorithm). **a** 0.4 unit ramp downward force with zero temperature, **b** restricted expansion under uniform ramp temperature rise to 40 C°, **c** downward ramp displacement of 0.4 units with zero temperature rise, **d** the coupling of the loading conditions of cases (b) and (c)

It is natural that the number of surface elements in the grinding zone plays an important role in solution accuracy. Therefore a careful selection of sufficient number of elements has been carried out. Figure 5 demonstrates the pattern of the consistent nodal forces during refining the mesh surface elements. It should be noted that more surface elements may have smoother variation of consistent nodal forces but at the cost of a much increased computation time. In this study, four surface elements were found to be sufficient.

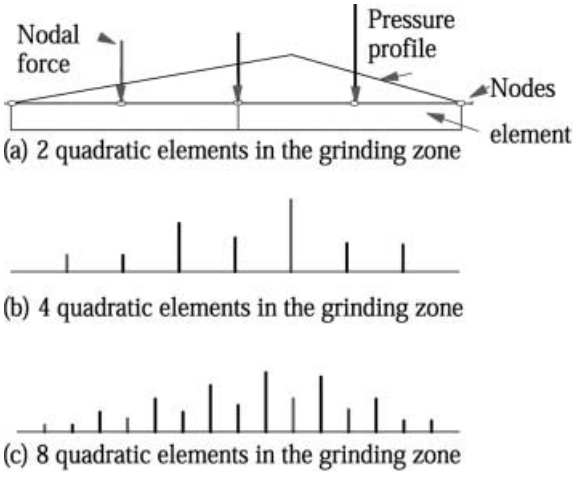

Fig. 5. The consistent nodal forces and FEM boundary mesh size

2.2.4 Thermo-mechanical coupling

Theoretically, the cooling to room temperature is a very slow process and thus needs a huge number of time steps. To resolve this dilemma (according to the authors' experience), it is assumed that after 80 time steps the grinding temperature reduces linearly in 20 time steps to room temperature ($T_\infty = 0$). Similarly, the moving traction intensity is reduced linearly to zero to approximate the simulation of the mechanical unloading action. To this end, the temperature file is scanned for each time step by reading the time and temperature at nodes. Then, a new temperature file is generated with modified temperature history. Here, the time step is considered to be the time required for the grinding forces in the grinding zone to cover the minimum distance between two surface nodes. For instance, according to the grinding condition of Pe = 1, workmaterial properties and the FEM mesh size specify that the time step is 0.0101396 s. However, it is necessary to ensure that the time step in thermal analysis, Δt, is unity so that it becomes consistent with that in the stress analysis. To achieve this, the equation of heat conduction of surface grinding

$$\kappa\left(\frac{\partial^2 T}{\partial x^2}+\frac{\partial^2 T}{\partial z^2}\right)=c\frac{\partial T}{\partial t} \tag{7}$$

needs to be modified to use a different time scale by altering the right hand terms such that the time step for

stress analysis is always unity. By employing a dimensionless time variable,

$$t^{-} = \frac{t\,\mathrm{Pe}}{\Delta t} \quad , \tag{8}$$

Eq. (7) can be rewritten as

$$\kappa\left(\frac{\partial^2 T}{\partial x^2} + \frac{\partial^2 T}{\partial z^2}\right) = \frac{c\mathrm{Pe}}{\Delta t}\frac{\partial T}{\partial t^{-}} \quad , \tag{9}$$

Letting

$$c^{-} = \frac{c\mathrm{Pe}}{\Delta t} \tag{10}$$

Eq. (9) can be further reformatted to

$$\kappa\left(\frac{\partial^2 T}{\partial x^2} + \frac{\partial^2 T}{\partial z^2}\right) = c^{-}\frac{\partial T}{\partial t^{-}} \quad . \tag{11}$$

A comparison of Eq. (7) with Eq. (11) indicates that Δt becomes unity when the new specific heat capacity per unit volume, c^{-} defined by Eq. (10), is used instead of c. Therefore to couple the thermal and mechanical analysis, Eq. (8) should be used.

The details of thermal and mechanical coupling are more clearly demonstrated in Fig. 6, which shows that in the way developed above the treatment of coupling requires a little effort at the joining parts of the algorithm as

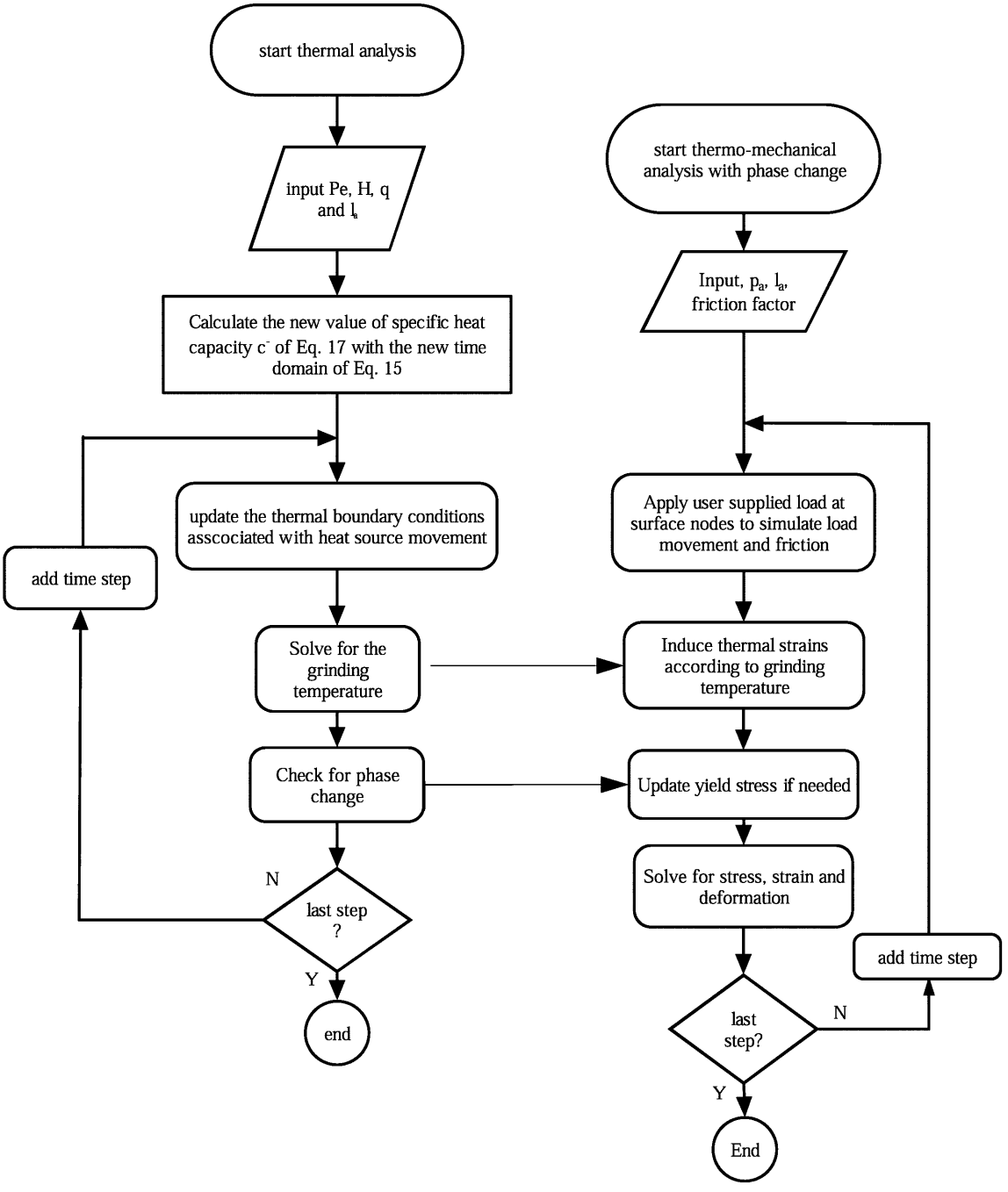

Fig. 6. The complete algorithm incorporating mechanical deformation, thermal deformation and phase transformation

the induction of grinding temperature into thermo-mechanical analysis and the updating of yield stress during phase change is independent of mechanical loading. As clearly shown above, the algorithm is explicit.

3 Application

The following is an example of application of the algorithm summarized in Fig. 6 to surface grinding with the full coupling of mechanical deformation, thermal deformation and phase transformation.

A control volume of the dimension of $24L_c \times 12L_c$ is selected for the analysis based on the criterion that boundary effects become negligible and grinding temperature becomes asymptotic, where L_c is the length of the contact zone between the grinding wheel and workpiece. The finite element mesh are shown in Fig. 7, where the subsurface layer is divided by 8 sets of thinner elements for modeling smoother change of workmaterial properties and residual stresses. The total number of elements and nodes in the control volume are 1248 and 5211 respectively.

As a central step in a thermo-mechanical analysis of grinding process, the initiation of irreversible deformation is a key factor in residual stress development. Therefore to initiate irreversible deformation in the workpiece, a critical coupling of thermal and mechanical grinding conditions that result in plastic deformation and phase transformation is essential. Figures 8–10 are the predictions of the critical conditions from the algorithm developed above.

Figure 8 reveals the onset of martensite transformation in relation to heat flux (HF) intensity. It is obvious that a higher convection heat transfer coefficient increases the input HF required to initiate the phase transformation. The critical input HF intensity is changing rapidly and can be considered as a power function of the Peclet number. To investigate critical thermo-mechanical grinding conditions, a large number of case studies is examined in Fig. 9. A typical condition of up-grinding ($l_a = 0.25$) is analyzed by varying the input HF intensity, q_a, the convection heat transfer coefficient, H, the Peclet number, Pe, the peak of the mechanical normal traction, p_a, and the 'friction' factor, μ. It is found that the 'friction' factor has a major role in decreasing the critical q_a and p_a (see Fig.9a).

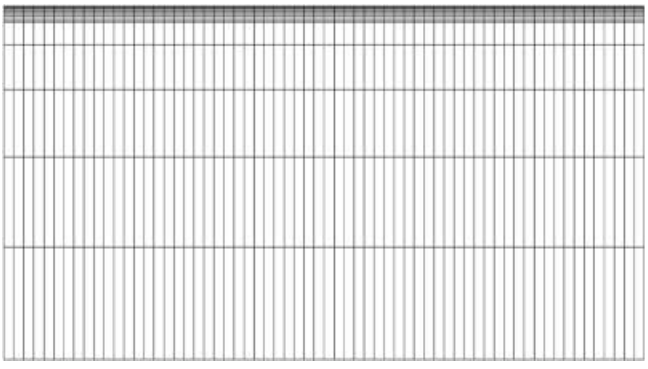

Fig. 7. Finite element mesh

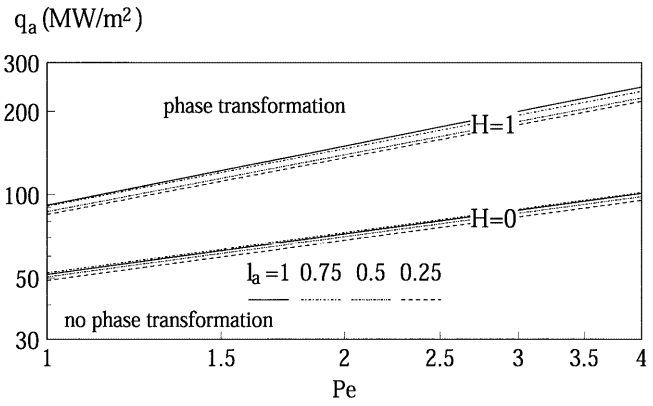

Fig. 8. Critical conditions of phase transformation

The critical q_a, increases as traction rises to a maximum near $p_a/Y = 0.2$ after which it decreases to a limit governed by the value of μ. It is also noted that a higher μ results in a lower critical p_a. It is interesting to note that plastic deformation may be developed at a lower HF intensity ($q_a < 5$ MW/m^2) but with high levels of normal traction. On the other hand, the convection heat transfer coefficient has a reversed role in affecting the critical grinding conditions as a higher H requires higher levels of critical q_a and p_a (see Fig. 9b) to generate the same grinding temperature rise. It is therefore clear that a higher q_a is needed to maintain the plastic deformation as grinding temperature decreases. Moreover, the critical heat flux intensity is proportional to the normal traction pressure profile to a limit, characterized by the sudden decrease of the critical q_a at about $p_a/Y = 1.1$ when $H = 1.0$.

It is also predicted that table speed has a similar role to that of the convection heat transfer coefficient since a higher table speed results in a lower grinding temperature if heat flux intensity is kept the same. Therefore higher Peclet numbers brings about higher levels of critical heat flux intensity to a limit of $p_a/Y = 1.1$.

The results shown in Fig.10 demonstrates that when a workpiece experiences a critical temperature variation in grinding, phase change occurs at a certain distance away from the grinding zone. It is clear that for the same maximum austenising temperature, phase change starts earlier if H is higher. Moreover, no cooling in the grinding zone ($w = 0$) or no cooling over the whole grinding surface ($H = 0$) decelerates the initiation of phase transformation.

When the grinding conditions become beyond the critical conditions, the surface residual stresses start to develop in a manner relying on the nature of thermal and mechanical loading coupling. For instance, the effect of cooling mechanism, traction and table speed on the distribution of residual stresses can be understood deeply by comparing the influence of the causes individually and with different combinations. Figure 11 shows the role of each mechanism of different grinding conditions on longitudinal residual stress, σ_{xx}. Under dry thermal conditions (case 1), a large residual stress is developed in the martensite zone. If convection cooling

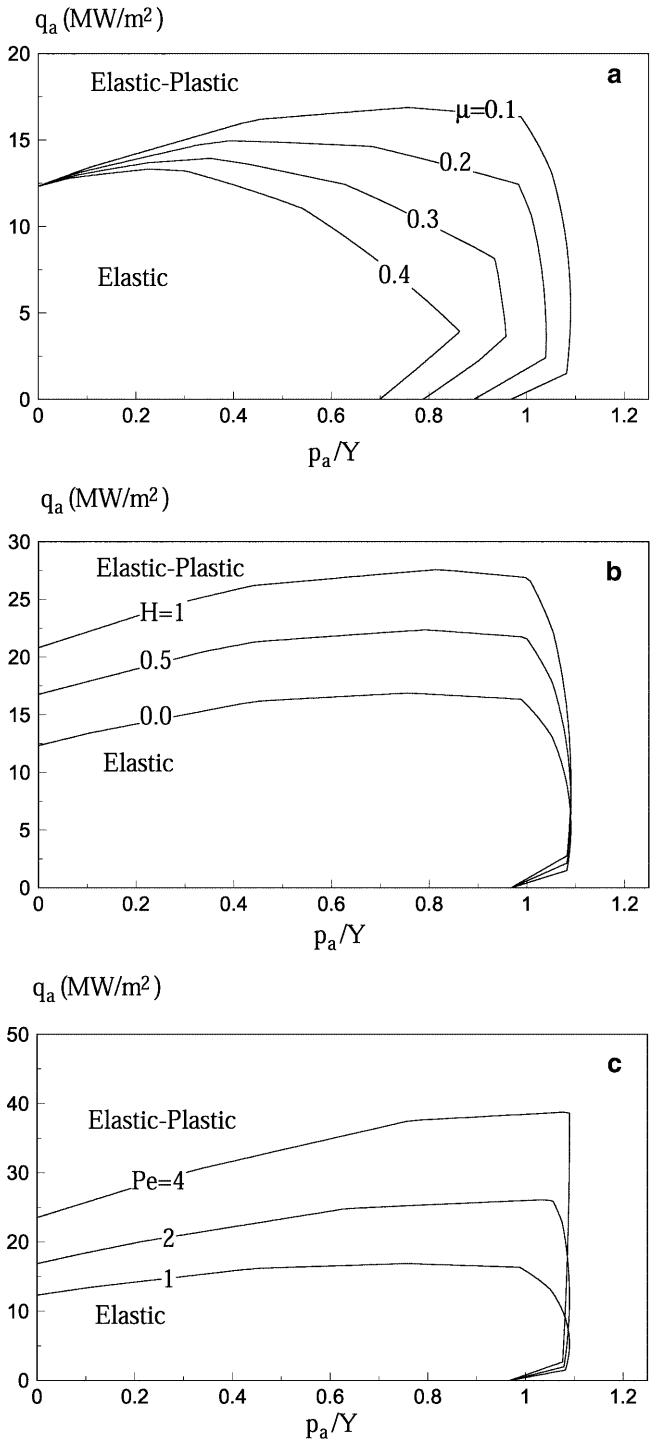

Fig. 9a–c. Critical thermo-mechanical grinding conditions ($l_a = 0.25$) **a** effect of 'friction' factor ($H = 0$, Pe = 1), **b** effect of convection heat transfer coefficient (Pe = 1, $\mu = 0.1$), **c** effect of Peclet number ($H = 0$, $\mu = 0.1$)

is applied (e.g. $H = 1$), no martensite is formed and the residual stresses are of thermo-mechanical conditions with constant workmaterial properties (cases 2–4). Under pure thermal grinding condition with uniform cooling (e.g. $H = 1, w = 1, p_a = 0$), the residual stresses are changing smoothly across the ground depth. If mechanical traction is imposed (case 3), the surface residual stress is reduced and its distribution becomes nearly a

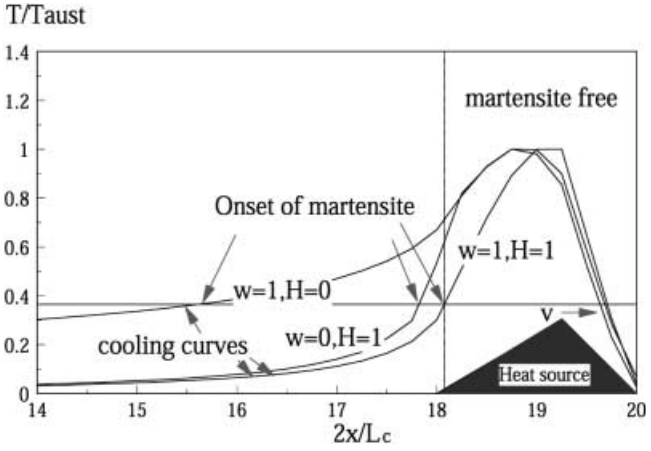

Fig. 10. Onset of phase change vs heat source location ($l_a = 0.25$)

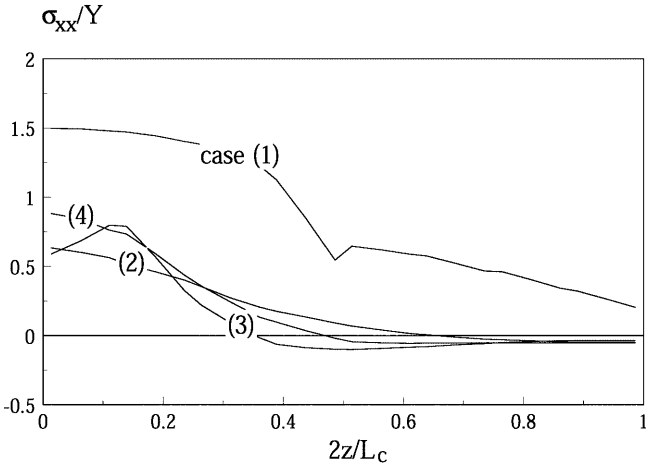

Fig. 11. Combined effect of cooling mechanism, traction and table speed on residual stress $\sigma_{xx}(l_a = 0.25, q_a = 80\,\mathrm{MW/m^2})$, case (1): ($H = 0$, Pe = 1, $p_a/Y = 2$), case (2): ($H = 1$, Pe = 1, $\mu = 0.3$, $w = 1$, $p_a/Y = 0$), case (3): ($H = 1$, Pe = 1, $\mu = 0.3$, $w = 1$, $p_a/Y = 2$), case (4): ($H = 1$, Pe = 4, $\mu = 0.3$, $w = 0$, $p_a/Y = 2$)

periodic decaying function of depth. At a higher table speed and no cooling in the grinding zone (Pe = 4, $H = 1$, $w = 0$) of case 4, the surface residual stress is increased and becomes smooth. The distribution of residual stress is similar to that of case 2. Therefore the mechanical traction has a certain role on residual stresses if uniform convection surface cooling and low Peclet number are maintained.

4 Conclusion

A numerical algorithm for treating the coupling of the thermo-mechanical analysis with phase transformation and the boundary conditions has been developed, tested and employed to investigate the practical cases of surface grinding. The application shows that this explicit algorithm is stable and efficient in dealing with the strong non-linearity associated with grinding. The numerical predictions offer some new insights into the mechanisms of critical grinding conditions.

Appendix

Under plane-strain conditions in xz-plane, the square of (von Mises) effective stress can be expressed as

$$\sigma_e^2 = \tfrac{1}{2}((\sigma_{xx}-\sigma_{zz})^2 + (\sigma_{xx}-\sigma_{yy})^2 + (\sigma_{yy}-\sigma_{zz})^2 + 6\sigma_{xz}^2) \quad \text{(A1)}$$

For given increments of stresses $\Delta\sigma_{xx}, \Delta\sigma_{zz}, \Delta\sigma_{yy}$ and $\Delta\sigma_{zx}$, the trial effective stress can be expressed as

$$\begin{aligned}\sigma_e^{\text{trial }2} = {} & \tfrac{1}{2}((\sigma_{xx}-\sigma_{yy}) + (\Delta\sigma_{xx}-\Delta\sigma_{yy}))^2 \\ & + \tfrac{1}{2}((\sigma_{xx}-\sigma_{zz}) + (\Delta\sigma_{xx}-\Delta\sigma_{zz}))^2 \\ & + \tfrac{1}{2}((\sigma_{yy}-\sigma_{zz}) + (\Delta\sigma_{yy}-\Delta\sigma_{zz}))^2 \\ & + 3(\sigma_{xz}+\Delta\sigma_{xz})^2 \end{aligned} \quad \text{(A2)}$$

If the trial effective stress exceeds the yield stress, Y, the stress increments should be scaled by a factor r, such that the intermediate effective stress, σ_e^{inter} be equal to the yield stress, Y, thus,

$$\begin{aligned}\sigma_e^{\text{inter }2} = Y^2 = {} & \tfrac{1}{2}((\sigma_{xx}-\sigma_{yy}) + r(\Delta\sigma_{xx}-\Delta\sigma_{yy}))^2 \\ & + \tfrac{1}{2}((\sigma_{xx}-\sigma_{zz}) + r(\Delta\sigma_{xx}-\Delta\sigma_{zz}))^2 \\ & + \tfrac{1}{2}((\sigma_{yy}-\sigma_{zz}) + r(\Delta\sigma_{yy}-\Delta\sigma_{zz}))^2 \\ & + 3(\sigma_{xz}+r\Delta\sigma_{xz})^2 \end{aligned} \quad \text{(A3)}$$

This equation can be rewritten as

$$\begin{aligned} Y^2 = {} & \tfrac{1}{2}\Big((\sigma_{xx}-\sigma_{zz})^2 + (\sigma_{xx}-\sigma_{yy})^2 + (\sigma_{yy}-\sigma_{zz})^2 \\ & + 6\sigma_{xz}^2) + r((\sigma_{xx}-\sigma_{zz})(\Delta\sigma_{xx}-\Delta\sigma_{zz}) \\ & + (\sigma_{xx}-\sigma_{yy})(\Delta\sigma_{xx}-\Delta\sigma_{yy}) \\ & + (\sigma_{yy}-\sigma_{zz})(\Delta\sigma_{yy}-\Delta\sigma_{zz}) + 6\sigma_{xz}\Delta\sigma_{xz}\Big) \\ & + r^2\Big((\Delta\sigma_{xx}-\Delta\sigma_{yy})^2 + (\Delta\sigma_{xx}-\Delta\sigma_{zz})^2 \\ & + (\Delta\sigma_{zz}-\Delta\sigma_{yy})^2 + 6\Delta\sigma_{xy}^2\Big)/2 \end{aligned} \quad \text{(A4)}$$

which can be further simplified to

$$\begin{aligned} Y^2 = {} & \sigma_e^2 + r\Big((\sigma_{xx}-\sigma_{zz})(\Delta\sigma_{xx}-\Delta\sigma_{zz}) \\ & + (\sigma_{xx}-\sigma_{yy})(\Delta\sigma_{xx}-\Delta\sigma_{yy}) \\ & + (\sigma_{yy}-\sigma_{zz})(\Delta\sigma_{yy}-\Delta\sigma_{zz}) + 6\sigma_{xz}\Delta\sigma_{xz}\Big) \\ & + r^2\Big((\Delta\sigma_{xx}-\Delta\sigma_{yy})^2 + (\Delta\sigma_{xx}-\Delta\sigma_{zz})^2 \\ & + (\Delta\sigma_{zz}-\Delta\sigma_{yy})^2 + 6\Delta\sigma_{xy}^2\Big)/2 \end{aligned} \quad \text{(A5)}$$

That is,

$$\begin{aligned} & \Big((\Delta\sigma_{xx}-\Delta\sigma_{yy})^2 + (\Delta\sigma_{xx}-\Delta\sigma_{zz})^2 + (\Delta\sigma_{zz}-\Delta\sigma_{yy})^2 \\ & + 6\Delta\sigma_{xy}^2\Big)/2r^2 + \Big((\sigma_{xx}-\sigma_{zz})(\Delta\sigma_{xx}-\Delta\sigma_{zz}) \\ & + (\sigma_{xx}-\sigma_{yy})(\Delta\sigma_{xx}-\Delta\sigma_{yy}) \\ & + (\sigma_{yy}-\sigma_{zz})(\Delta\sigma_{yy}-\Delta\sigma_{zz}) \\ & + 6\sigma_{xz}\Delta\sigma_{xz}\Big)r + \sigma_e^2 - Y^2 = 0 \end{aligned} \quad \text{(A6)}$$

This shows that, r is the root of

$$c_1 r^2 + c_2 r + c_3 = 0 \quad \text{(A7)}$$

where

$$\begin{aligned} c_1 = {} & \tfrac{1}{2}\Big((\Delta\sigma_{xx}-\Delta\sigma_{zz})^2 + (\Delta\sigma_{xx}-\Delta\sigma_{yy})^2 \\ & + (\Delta\sigma_{yy}-\Delta\sigma_{zz})^2 + 6\Delta\sigma_{xz}^2\Big) \\ c_2 = {} & \Big((\Delta\sigma_{xx}-\Delta\sigma_{zz})(\sigma_{xx}-\sigma_{zz}) \\ & + (\Delta\sigma_{xx}-\Delta\sigma_{yy})(\sigma_{xx}-\sigma_{yy}) \\ & + (\Delta\sigma_{zz}-\Delta\sigma_{yy})(\sigma_{zz}-\sigma_{yy}) + 6\sigma_{xz}\Delta\sigma_{xz}\Big) \\ c_3 = {} & (\sigma_e^2 - Y^2) \end{aligned} \quad \text{(A8)}$$

The roots of Eq. (A7) are

$$\begin{aligned} r_1 &= (-c_2 + (c_2^2 - 4c_1c_3)^{1/2})/(2c_1) \quad \text{and} \\ r_2 &= (-c_2 - (c_2^2 - 4c_1c_3)^{1/2})/(2c_1) \end{aligned} \quad \text{(A9)}$$

References

ADINA R & D, Inc. (1992) Theory and modelling guide. Report ARD 92-5, ADINA R & D, Inc.

Atkin M, Met B (1977) Atlas of Continuous Cooling Transformation diagrams for Engineering Steels. Market Promotion Department, British Steel Corporation, BBC Billet, Bar and Rod Products, Sheffileld, UK

Bathe K-J (1982) Finite Element Procedures in Engineering Analysis. Prentice-Hall

British Iron and Steel Research Association (1969) The Mechanical and Physical Properties of the British Standard on Steels, vol. 2. Pergamon Press, Oxford, UK

Kim W-B, Na S-J (1992) Study on residual stresses in surface hardening by high frequency induction heating. Surface and Coatings Technol. 52/3: 281–288

Mahdi M, Zhang L (1994) Correlation between grinding conditions and phase transformation of an alloy steel. In: Wrobel LC et al. (eds) Advanced Computational Methods in Heat Transfer, III: pp. 193–200. Computational Mechanics Publications. Southampton

Mahdi M, Zhang L (1995) The finite element thermal analysis of grinding processes by ADINA, Comp. Struct. 56: 313–320

Mahdi M, Zhang L (1996) A Theoretical Investigation on the Mechanically Induced Residual Stresses due to Surface Grinding. In: Narutaki N et al. (eds) Progress of Cutting and Grinding, III: pp. 484–487. Japan Society for Precision Engineering, Osaka

Mahdi M, Zhang L (1997) Applied mechanics in grinding, Part V: thermal residual stresses. Int. J. Machine Tools and Manufact. 37: 619–633

Mahdi M, Zhang L (1998a) Applied mechanics in grinding, Part VI: residual stresses and surface hardening by coupled thermo-plasticity and phase transformation. Int. J. Machine Tools and Manufact. 38: 1289–1304

Mahdi M, Zhang L (1998b) Residual stresses in ground components: effect of thermo-mechanical deformation. Proceedings of the 4th International Conference on Progress of Cutting and Grinding, pp. 447–452. Japan Society for Precision Engineering, Beijing

Mahdi M, Zhang L (1999) Applied mechanics in grinding, Part 7: residual stresses induced by the full coupling of mechanical deformation, thermal deformation and phase transformation. Int. J. Machine Tools and Manufact. 39: 1285–1298

Nakasaki K, Inoue T (1997) Metallo-thermo-mechanical simulation of laser-quenching process of carbon steel by pulsed YAG laser beam. Zairyo/J. Soc. Materials Sci. Japan 46/3: 268–275

Okamura K, Kawashima H (1989) Numerical analysis of residual deformation of a gear ring during quenching. Sumitomo Metals 41/4: 11–18

Taljat B, Radhakrishnan B, Zacharia T (1998) Numerical analysis of GTA welding process with emphasis on post-solidification phase transformation effects on residual stresses. Materials Sci. Eng. A: Struct. Materials: Properties, Microstructure and Processing A246/1–2: 45–54

Zhang L, Mahdi M (1995) Applied mechanics in grinding, Part IV: the mechanism of grinding induced phase transformation. Int. J. Machine Tools and Manufact. 35: 1397–1409